LEMRAP Laboratory
2022 Annual report

R. Bedogni (Responsabile), C. Cantone
A. Pietropaolo (Associato), J-M Gomez-Ròs (Associato)
A. Calamida (Assegnista), L. Russo (Borsista)
I.A. Castro Campoy (Ospite ICTP), A. Fontanilla (Ospite ICTP)
In collaboration with
INFN- LNF Servizio Progettazione e Costruzioni Meccaniche
Torino University and INFN section
ENEA Frascati

1 ENTER_BNCT experiment (2020 - 2022) - CSN 5

1.1 Introduction

Neutron Capture Therapy (NCT) is an alternative form of radiotherapy based on neutrons with energy in the keV-tens keV region (epithermal neutrons). The tumour cells are not directly killed by neutrons impinging the patient, but through a "sensitizer" agent in the form of a drug with the following main characteristics:

- Designed to ideally reach only malignant cells;
- Contains a high percentage of elements with high neutron interaction probability, or more precisely high neutron capture cross section;
- This neutron absorbing material produces secondary ionising radiations as a result of the neutron capture, having the capability to kill the surrounding malignant cells. this preferentially occurs in the thermal neutron domain;
- The secondary particles are preferably charged particles with energy in the order of MeV and range in the order of few to ten μm in tissue, so that the killing effect is limited to the labelled cell and the damage to surrounding healthy cells is limited.

Of the elements with highest thermal neutron capture cross-section, like ^{3}He, Cd, ^{10}B, ^{6}Li or Ga, only Ga and ^{10}B have been studied for NCT as they are practicably usable to mark pharmaceutical drugs. Gadolinium has higher cross section but the secondary particles, electrons and gammas, are weakly ionising if compared to the charged particles produced in the reaction ^{10}B(n,α)^{7}Li. Being ^{10}B the best candidate for NCT, this type of therapy is also called BNCT (*Boron Neutron Capture Therapy*).

Current scientific challenges in BNCT are:

- Designing a drug that maximises the ratio between the Boron concentration in the tumour and that in the surrounding normal tissues (Boron uptake);
- Maximising the thermal neutron fluence rate in the tumour location.

As the human body is mainly water, it slows-down neutrons and tend to absorb them when they reach thermal energies. Thus a thermal neutron beam would be effective only for superficial tumours. By contrast, deep-seated tumours (up to about $6 \div 8$ cm) require epithermal neutrons: after being slowed-down in the surrounding tissues, they will reach the tumour with energy in the thermal domain. Neutron sources for BNCT are nuclear reactor or particle accelerators coupled with a neutron producing target. Primary neutrons have MeV energies. A beam shaping assembly

(BSA) is used to degrade the energy distribution of the primary neutrons to achieve the desired epithermal spectrum.

Spectrometric techniques would be very desirable in BNCT, but are not currently implemented as neutron spectrometers are usually very complex and unsuited for routine scenarios. Also, very few neutron spectrometers simultaneously cover from thermal to MeV in energy. Bonner spheres fulfil this requirement, but they are cumbersome and do not work in real time. In addition, most existing neutron detectors do not operate in the very intense therapeutic fields encountered in BNCT.

The ENTER_BNCT project aims to develop technical and measurement capabilities for the implementation of a centre for clinical BNCT based on a particle accelerator. The project involves four INFN units: Pavia, Turin, LNL and LNF. The main objectives of the project are:

- Developing a beryllium neutron target (LNL);
- Developing a Beam Shaping Assembly (made up of a new materials developed in previous project BEAT_PRO (Pavia);
- Design of the irradiation room and related tools (Pavia);
- Boron concentration measurements for clinical application (evaluations in the blood to determine irradiation time) and intra-cellular evaluation of boron distribution to calculate more precise dosimetry parameters (Pavia);
- Development of new neutron spectrometer able to work as routine tool for beam control in BNCT, called NCT-WES (*Neutron Capture Therapy - Wide Energy Spectrometer*) (LNF+Torino).

1.2 The NCT-WES neutron spectrometer

NCT-WES is a new type of real-time neutron spectrometer able to work as routine tool for beam control in BNCT. It is a single-moderator-type spectrometer based on a collimated cylindrical structure, see Fig. (1).

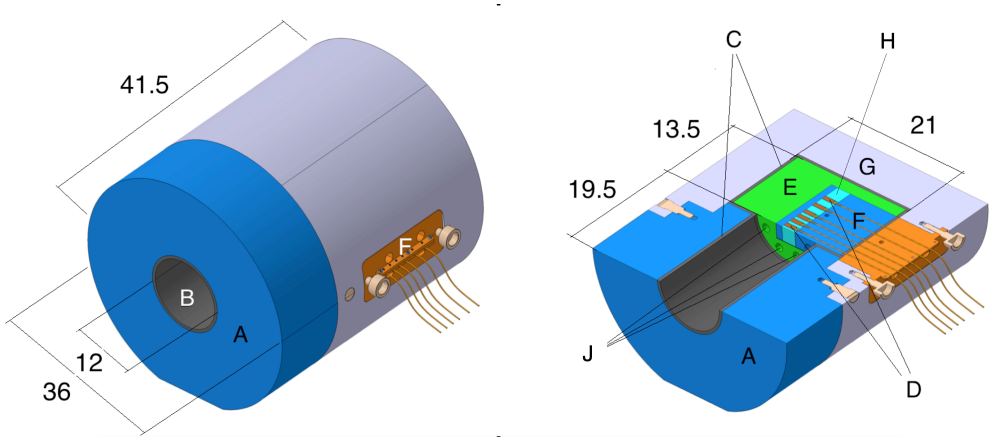

Figure 1: Schematics of the NCT-WES spectrometer. Quotes are in cm.

NCT-WES appears as a HDPE (high-density polyethylene) cylinder with diameter 36 cm and total length 41.5 cm. The dimensions of the cylinder as well as the location of detectors have been

chosen to maximize the "spectrometric capability" of the device in the epithermal domain, i.e. the degree of differentiation between the response functions associated to different detector positions. The collimator, label A in Fig. (1), is 19.5 cm in length and its collimating aperture (label B), 12 cm in diameter, is internally lined with 0.5 cm of borated plastic SWX-238 from Shieldwerx (label C). Six thermal neutron detectors (D), located along the cylindrical axis, are contained in the HDPE capsule (label E, 20 cm in diameter, 13.5 cm in length). In order to facilitate maintenance, they are embedded in an extractable HDPE drawer (label F + label H). An external shield made of 0.5 cm of SWX-238 (label C) plus 7.5 cm of HDPE (label G) protects the capsule against neutrons arising from undesired directions. The centre of the shallowest detector is located at 0.72 cm depth from the end of the collimator. Detectors spacing (centre to centre) is 1.3 cm from the 1st to the 4th, and 2 cm from the 4th to the 6th. The detectors, called TNPDs (*Thermal Neutron Pulse Detector*), are parallelepipeds with external dimensions $0.32 \times 1.5 \times 1.3$ cm^3 and are connected through a 2 mm diameter coaxial cable. It should be noted that NCT-WES can be adapted to allocate internal detectors with different size by simply replacing the polyethylene piece labelled H.

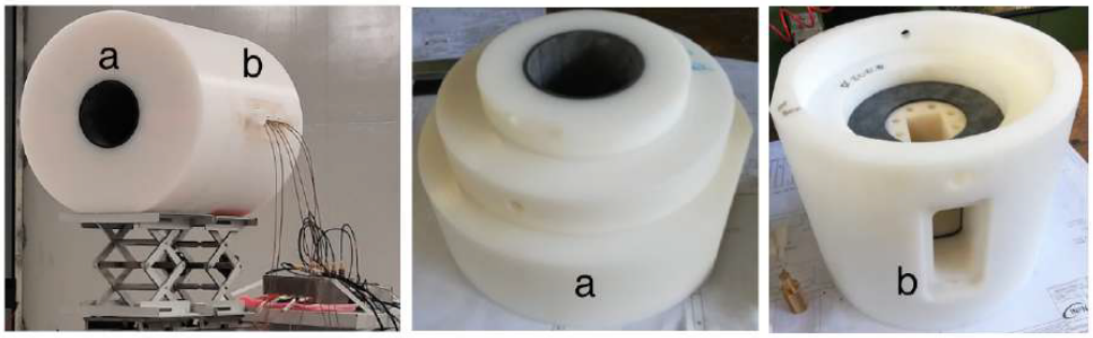

Figure 2: NCT-WES. On the left, the assembled prototype with the detector drawer inserted. At the centre, the part (a) including the collimator. On the right, the part (b) including the sensitive the capsule and its lateral protection. Air penetrations are visible. The drawer is extracted.

Label J refers to eight cylindrical air cavities, 1.3 cm in diameter, designed to enhance the response of deeper detectors relying on neutron streaming. The centres of these cavities are equally spaced on a circumference with radius 4.25 cm centred on the NCT-WES cylindrical axis. The assembled NCT-WES is shown in Fig. (2).

A Monte Carlo model was done to obtain the response matrix, obtaining the result in Fig. (3).

1.3 Validation with monoenergetic epithermal beams

Although NCT-WES response was already validated in a reference ^{241}Am-Be field, additional validation measurements in monoenergetic epithermal fields are required, in view of its use in BNCT. The validation experiment described in this work was organized at the NPL (*National Physical Laboratory*) of Teddington UK and involved the following reference monoenergetic fields: 71.5 keV, 144.2 keV, 565.1 keV, 841.9 keV and 1200.4 keV.

The irradiation tests took place in the low-scatter irradiation room of NPL, using the 3.5 MV Van de Graaff accelerator operated by the Neutron Metrology Group. The distance from the target to the front face of NCT-WES, henceforth indicated as *SDD* (*Source to Detector Distance*) ranged from 180 to 230 cm. The shadow-cone technique was used to subtract the air- and room-scatter

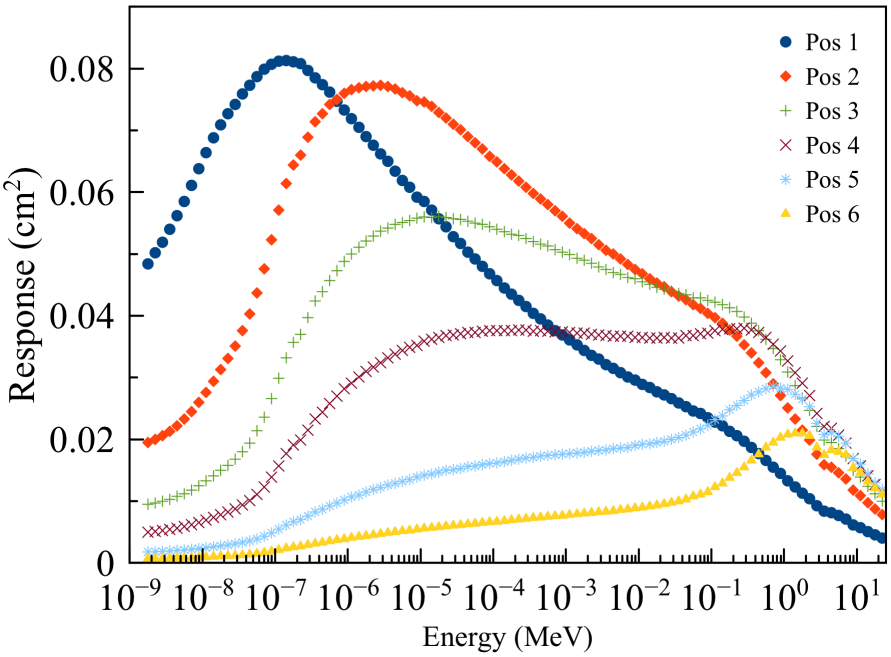

Figure 3: NCT-WES response matrix. The response is the expected number of measurable pulses in the TNPD, per unit incident fluence, as a function of the energy and the detector position.

contribution from the spectrometer readings. The set up can be seen in Fig. (4). The reference value of monoenergetic neutron fluence delivered to the reference point (front face of NCT-WES) was known from measurements performed by means of the Standard NPL long counter in addition to a suite of permanent monitor instruments. The main characteristics of the used beams are summarized in Tab. (1). The *Target Scatter Fraction* (*TSF*), based on Monte Carlo simulations carried out at NPL, can be assumed as affected by uncertainty up to ±40% [1)]. These are neutrons with lower energy than the monoenergetic ones. Since the long counter used to determine the reference fluence has flat energy dependence of the fluence response, then the result is a slight overestimation of the monoenergetic fluence. The signals from the TNPD detectors are recorded using a custom six-channel analogue board, each channel including a charge preamplifier of type CREMAT CR-110 and a shaper amplifier of type CREMAT CR-200 with time constant 2 μs. As a method to reduce the noise in the analogue signal, detectors are inversely biased to 12 V. According to dedicated C-V measurements, this corresponds to a junction capacitance of about 100 pF. Its impact on the amplified signal noise is only $4 \div 5$ mV RMS. This is very small, if compared to the amplitude of the neutron signals. The genuine neutron-induced events are discriminated from those induced by photons by comparing the pulse height with a threshold, fixed at 0.6 V. The neutron-induced pulse height distribution (PHD) in the TNPD extends in amplitude from this threshold up to about 3 V, with an energy-pulse amplitude conversion factor of about ~ 1 V·MeV^{-1}. A commercial digitizer (NI USB 6366), operating in streaming mode under customized software written in LabView, allows the data to be recorded on a laptop. The "neutron counts" of each TNPD were obtained by integrating the PHD from 0.6 V to 3 V.

For a given monochromatic irradiation, the measured NCT-WES response, R_m, was derived

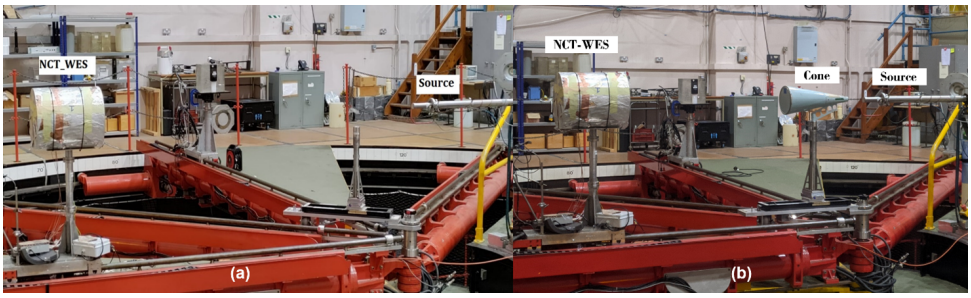

Figure 4: The experimental set-up in the low-scatter irradiation room of NPL. The shadow-cone is in place.

Table 1: Irradiation conditions: E_n is the monochromatic neutron energy, R the reaction, u_φ is the standard uncertainty on the neutron fluence at SDD, TSF is given as a percentage of the total fluence

E_n (MeV)	$FWHM$ (keV)	R	Angle (deg)	u_φ	TSF	SDD (cm)
71.5 ± 4.2	26	^{7}Li(p,n)	50	$\pm 4.4\%$	1.7%	180.7
144.2 ± 4.6	29	^{7}Li(p,n)	0	$\pm 2.9\%$	1.1%	181.0
565.1 ± 3.6	19	^{7}Li(p,n)	0	$\pm 2.7\%$	0.6%	230.8
841.9 ± 11.6	77	T(p,n)	50	$\pm 2.3\%$	$< 3.6\%$	180.6
1200.4 ± 14.8	98	T(p,n)	0	$\pm 2.3\%$	3.6%	180.7

for every detector, as follows:

$$R_m = \frac{C_{i,tot}}{N_{tot}} - \frac{C_{i,cone}}{N_{cone}}, \tag{1}$$

With $C_{i,tot}$ and $C_{i,cone}$ the neutron counts (integrated between $0.6 \div 3$ V) for the detector in the i-th position in the total field and shadow-cone irradiations respectively, N_{tot} and N_{cone} the number of monoenergetic neutrons emitted by the target if the emission was isotropic.

Clearly the monoenergetic neutron emission from a target is not isotropic in terms of fluence or energy. Nevertheless, the NCT-WES collimator has a 12 cm diameter and is positioned at about 2 m form the target. Thus, the subtended solid angle is so small that the neutron field across this surface can be considered uniform in fluence and energy.

N_{tot} and N_{cone} are calculated by:

$$N = \Phi \cdot (1 - TSF) \cdot 4\pi \cdot SDD^2, \tag{2}$$

Where Φ is the neutron fluence.

The R_m values for the studied monoenergetic beams are reported in Table 2, where the R_s/R_m quotient, q, is also reported. A good agreement between simulation and experiment was obtained, the q values always being compatible with one (uncertainties are 1 standard deviation). The thirty values of $q_{i,E}$ (where i denotes the detector position and E the monoenergetic energy) are scattered with a s.d. of about 4%. If they are combined in a weighted mean, using the inverse square of uncertainties as weights, the best estimation of q is $q_{best} = (1.002 \pm 0.008)$. If the matrix given in Table 2 is analysed per columns, a weighted mean over the position can be calculated. The resulting q_E values, reported in the end of each column, are energy-dependent. All q_E values are very near to one, denoting no systematic errors depending on the energy. If for example the fluence monitoring was affected by a bias in a specific energy, the corresponding q value could

Table 2: NCT-WES response in terms of counts per emitted neutron as a function of the neutron energy and the detector position: simulated (R_s), measured (R_m) values, and their ratio q. Energy and position average q values are also reported.

	E (keV)	71.5	144.2	565.1	841.9	1200.4	q_i
	SDD (cm)	180.7	181.0	230.8	180.6	180.7	
	$R_s(\times 10^{-8})$	5.13 ± 0.33	4.96 ± 0.20	2.25 ± 0.07	3.15 ± 0.10	2.80 ± 0.09	
	$R_m(\times 10^{-8})$	4.85 ± 0.22	4.43 ± 0.14	2.20 ± 0.06	3.07 ± 0.08	2.79 ± 0.07	
P1	q	1.06 ± 0.08	1.06 ± 0.06	1.02 ± 0.04	1.03 ± 0.04	1.00 ± 0.04	1.03 ± 0.02
	$R_s(\times 10^{-8})$	8.53 ± 0.56	8.03 ± 0.34	4.05 ± 0.11	5.79 ± 0.18	5.17 ± 0.16	
	$R_m(\times 10^{-8})$	8.22 ± 0.37	7.69 ± 0.24	4.08 ± 0.12	5.78 ± 0.15	5.13 ± 0.13	
P2	q	1.04 ± 0.08	1.04 ± 0.05	0.99 ± 0.04	1.00 ± 0.04	1.01 ± 0.04	1.01 ± 0.02
	$R_s(\times 10^{-8})$	9.0011 ± 0.59	8.75 ± 0.37	4.82 ± 0.14	7.03 ± 0.22	6.38 ± 0.20	
	$R_m(\times 10^{-8})$	8.53 ± 0.39	8.14 ± 0.25	4.68 ± 0.13	6.79 ± 0.17	6.31 ± 0.16	
P3	q	1.06 ± 0.08	1.07 ± 0.06	1.03 ± 0.04	1.04 ± 0.04	1.01 ± 0.04	1.03 ± 0.02
	$R_s(\times 10^{-8})$	7.73 ± 0.50	7.88 ± 0.33	4.80 ± 0.13	7.23 ± 0.23	6.72 ± 0.21	
	$R_m(\times 10^{-8})$	7.78 ± 0.35	7.77 ± 0.24	5.04 ± 0.14	7.41 ± 0.19	7.10 ± 0.18	
P4	q	0.99 ± 0.08	1.01 ± 0.05	1.98 ± 0.04	0.98 ± 0.04	0.95 ± 0.04	0.97 ± 0.02
	$R_s(\times 10^{-8})$	4.77 ± 0.31	5.17 ± 0.22	3.82 ± 0.11	6.10 ± 0.19	5.98 ± 0.18	
	$R_m(\times 10^{-8})$	4.63 ± 0.21	4.93 ± 0.15	3.86 ± 0.11	5.84 ± 0.15	5.81 ± 0.15	
P5	q	1.03 ± 0.08	1.05 ± 0.06	0.99 ± 0.04	1.04 ± 0.04	1.03 ± 0.04	1.03 ± 0.02
	$R_s(\times 10^{-8})$	2.53 ± 0.17	2.90 ± 0.212	2.56 ± 0.07	4.36 ± 0.14	4.52 ± 0.14	
	$R_m(\times 10^{-8})$	2.74 ± 0.13	3.00 ± 0.09	2.75 ± 0.08	4.40 ± 0.11	4.69 ± 0.12	
P6	q	0.92 ± 0.07	0.96 ± 0.05	10.99 ± 0.04	0.99 ± 0.04	0.96 ± 0.04	0.96 ± 0.02
	q_e	1.01 ± 0.03	1.03 ± 0.02	0.984 ± 0.016	1.011 ± 0.017	0.991 ± 0.016	

significantly deviate from one for that energy. If the matrix is analyzed per rows, a weighted mean over the energy is achieved. The resulting q_i values, reported in the end of each row, are position-dependent. Compared to the q_E values, the q_i values are more scattered. This depends on small detector-to-detector differences in terms of thermal neutron efficiency, or amount of ^{6}LiF radiator coating. However, being these deviations always lower or equal to 2σ, no detector-specific correction will be applied. Thus, the NCT-WES simulation model proved to be very accurate and its overall uncertainty, studied as a function of the energy or detector position, is always lower or equal to $\pm 2\%$.

2 SAMADHA (CSN 5)

2.1 Introduction

The SAMADHA project aims to investigate and study the neutron dose due to secondary neutrons produced by the interaction of cosmic particles with Oxygen and Nitrogen in atmosphere reaching the Earth below the SAA (*South Atlantic Anomaly*), a region in the planet with the lowest geomagnetic field where few or no data are available. This dose account for about one half of the effective dose received by humans at high-altitudes (i.e. commercial flights $5000 \div 7000$ m). Ambient dosimetry campaigns will be performed in high altitude sites in the SAA area, to study the relation between dose rate and space weather/atmospheric phenomena particularly at the high-altitude Chacaltaya Lab (5240 m) Bolivia. Neutron spectrometry using a new spectrometer designed specifically for the measurement of cosmic neutrons will be done to provide an accurate neutron dose assessment and obtain information on the factors affecting the dose contributions such as environmental conditions.

The SAMADHA research group consists of multidisciplinary experts from dosimetry, cosmic ray physics, solar physics, space weather atmospheric physics, with experience in instrumentation

and data analysis. INFN-LNF LEMRAP is one of the 5 collaborating groups and is responsible for:

- Design and construction of a Bonner sphere neutron spectrometer for measurements at high elevation;
- Ancillary systems for unattended operations;
- Monitor and data acquisition software;
- Data analysis and simulations.

The Bonner sphere spectrometer was completely built, characterised and calibrated in reference secondary standard field of ^{241}Am-Be (Politecnico di Milano), their diameter are:

- 80 mm;
- 100 mm;
- 120 mm;
- 150 mm;
- 170 mm;
- 200 mm;
- 200 with lead-bullets insert (apparent density of bullets $\rho \simeq 6.758$ g/cm^3);
- 200 with iron-bullets insert (apparent density of bullets $\rho \simeq 4.8094$ g/cm^3).

The internal metal parts in lead or iron (steel) are needed to increase the response above 10 MeV. A "fluid" filling made of metal bullets is cheaper than solid inserts, and can be purchased at low cost near the final destination of the spectrometer, thus reducing the shipping costs.

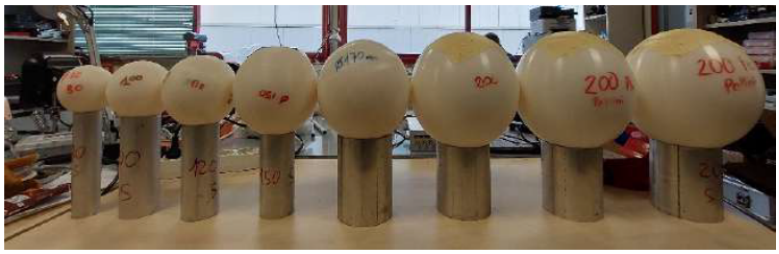

Figure 5: Bonner spheres of the SAMADHA spectrometer.

After manufacturing, the spheres where mechanically characterised in terms of actual sizes and density of all parts, and a very realistic MC (*Monte Carlo*) modelling of their response was performed, see Figs. (5). and (6).

The response functions for the SAMADHA spheres were simulated using the MCNP6 code for an extended neutron incidence energy range (from 1 meV to 5 GeV) to cover thermal to cosmic neutron energies. A set of 130 logarithmic equidistant discrete energy bins were chosen for each detector-sphere assembly. Fig. (6) shows the detailed model of the SAMADHA spectrometer based on the actual dimensions and composition of each sphere and the specifications of the ^{3}He detector provided by the manufacturer. For spheres with Pb and Fe balls inserts, their density is

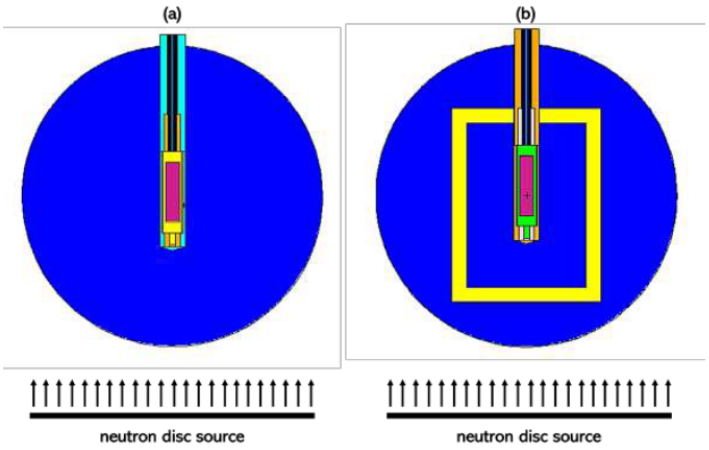

Figure 6: MC models used to simulate the response matrix of: (a) Spheres 80, 100, 120, 150, 170 and 200; and (b) Sphere 200 with Fe balls and Sphere 200 with Pb balls.

taken to be $\sim 60\%$ of the theoretical densities of solid Pb and Fe, respectively, to account for the air gaps that were not filled in when using the metal balls. The source, modelled as a disc with the same dimension as the spheres being irradiated, emits parallel neutron beams to the sphere. Simulations were performed using the Bertini cascade and Dresner evaporation models with the RAL fission model. The ENDF/B VIII.0 nuclear data libraries and its corresponding thermal neutron scattering $S(\alpha, \beta)$ data were also employed in all the calculations. The h-poly.80t used in the code accounted for thermal neutron scattering by hydrogen bound in polyethylene. The F4 tally was used in the simulations to derive the neutron fluence as a function of energy within the active volume of the ^{3}He detector. The response is expressed in terms of the number of (n, p) reactions for ^{3}He per unit fluence as a function of energy. The response matrix for all the sphere-detector configuration of the SAMADHA spectrometer is shown in Fig. (7). From the response functions, the system can completely characterize the energy distribution of the neutrons in a very large energy range. It can be observed that the maximum response, presented by the peak of the response functions, shifts from lower to higher energies with increasing sphere diameter. Large shift to higher energies for the large spheres is attributed to neutron thermalization in the sphere. Lower response function at the high energies is also evident due to elastic scattering with hydrogen in polyethylene. Spheres with the high-Z material inserts were also efficient in measuring neutrons above 20 MeV.

2.2 The Cervinia experimental campaign

After the calibration campaign and the final assembly of the system, an experimental campaign was carried on at Plateau Rosà in the Testa Grigia Laboratory to test the correct functioning of the spectrometer.

A major cause of error for this measurement is the presence of "spurious" signals, these are signal that can be confused as genuine neutron signals but they are only EM noise. An extensive study was conducted to identify and minimise these sources of "spurious" pulses in the detectors, i.e. due to other causes than incident neutrons, such as electromagnetic interferences or spikes in the supply lines. It was found that:

- Compared to the conventional coaxial cabling of the ^{3}He detectors, triaxial cabling of the ^{3}He detectors prevents spurious pulses due to electromagnetic interferences;

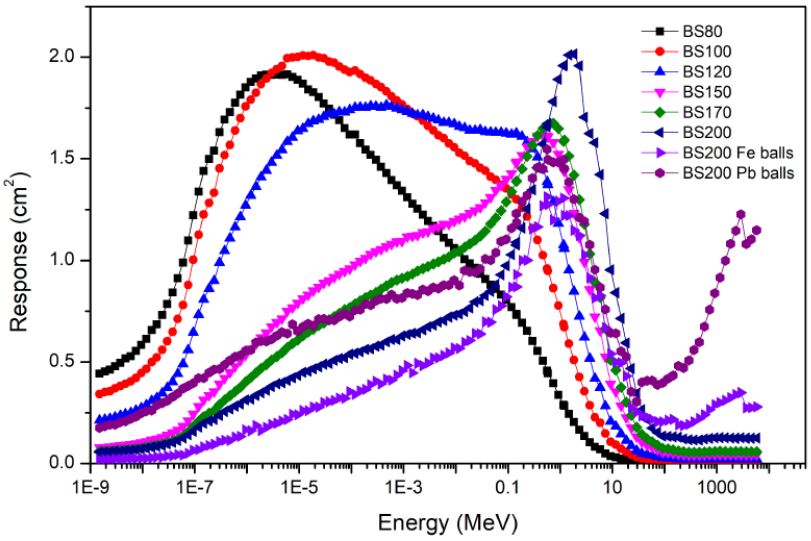

Figure 7: SAMADHA spheres response matrix calculated using the MCNP code.

- The high voltage generator (+850 V) is the major cause of spurious pulses and so, a massive capacitor-based filter on the high voltage output was applied;
- The low voltage generator (dual ±12 V) is the second cause of spurious pulses and so a massive capacitor-based filter on the low voltage output was applied;
- The stability of the 220 Vac line is the third cause of of spurious pulses, this was reduced by applying an UPS.

In addiction the following features were implemented in the LabView acquisition program:

- Gamma events are rejected by applying a lower threshold in pulse amplitude, set to 0.3 MeV;
- Small discharges in the detector may occur due to electronegative impurities in the filling gas or imperfections in the insulating materials, these discharges, resulting in pulses with amplitude higher than 1 V, are rejected by applying an upper threshold in pulse amplitude;
- The Fourier transformation is estimated for each signal and compared with the "reference one" calculated from a true genuine neutron signal.

The system was exposed at the Testa Grigia station for 15 hours starting from 13^{th} July 2022 at 18:00. The station is on a glacier with a large snow cover. According to Brall [4], the CFG (*Cosmic Field at Ground*) neutron fluence decreases with the snow cover, down to a factor of about 2.5 as compared to a soil without snow. Correspondingly, the cascade-to-evaporation peak ratio increases. The spectrometer was installed in a 3×6 m^2 room inside a one-floor building. The infrastructure includes internet access, which allows remote control of all parameters of the system. Various meteorological parameters are being measured on a routine basis, including the air pressure. The air pressure varied of less than 0.2% during the measurement time, with an average value of $\sim$ 681.9 hPa. The average count rates of the spectrometer are reported in Fig. (8) as a function of the diameter. The smooth shape of this curve indicates that the measurements were performed under "stable conditions", using the right monitors, and are not affected by supplementary uncertainties

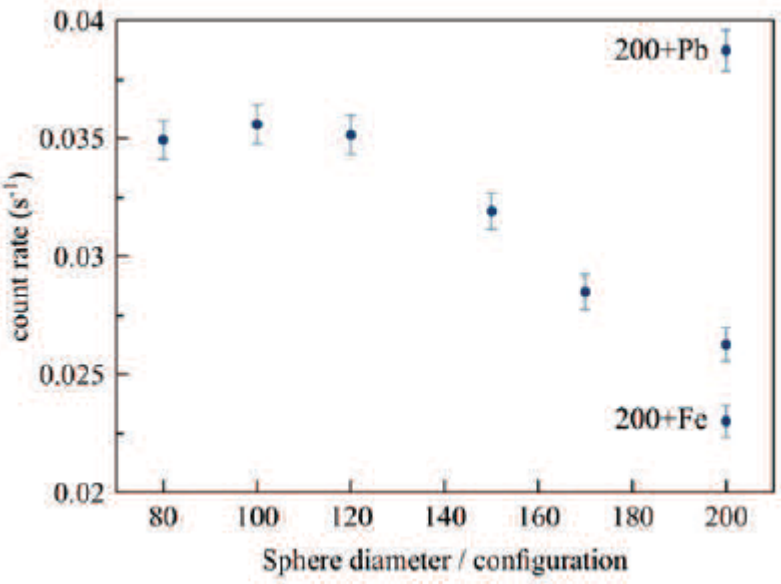

Figure 8: Average count rates of the Bonner Spheres spectrometer as a function of the diameter/sphere configuration.

of unexplained origin. This serves as a "consistency check", prior to the unfolding process. The count rates of Fig. (8) were unfolded with the FRUIT unfolding code [2), 3)], using the previously derived response matrix. The response functions were assumed to be affected by the following uncertainties:

- ±3% [5)] for the polyethylene spheres, mainly responding below 20 MeV where the cross sections are well-known;
- ±10% for the extended range spheres, mainly responding above 20 MeV where the cross sections are generated by model and affected by larger uncertainties [6), 7)].

Different guess-spectra were used to verify the robustness of the solution. As the presence of snow is recognized to be the main responsible for the shape of the spectrum, two unfolding sessions were conducted, using two guess spectra calculated by Brall *et al.* [4)] shown in Fig. (9).

Table 3: Spectrum-integrated quantities for the neutron component of the CFG at Testa Grigia station after correction for the atmospheric pressure and the solar activity.

Total fluence rate ($cm^{-2}{\cdot}s^{-1}$)	0.113 ± 0.013
Cascade fluence rate ($E < 20$ MeV, $cm^{-2}{\cdot}s^{-1}$)	0.049 ± 0.010
Total $H^*(10)$ ($\mu Sv{\cdot}h^{-1}$)	0.077 ± 0.011

As demonstrated in Fig. (10), the spectra obtained in the two separate unfolding sessions do not depend on the specific guess spectrum and provide the same output spectrum within unfolding uncertainties. This unfolded spectrum has a large cascade-to-evaporation peak ratio which is coherent with a large snow cover at the measurement site. The uncertainties in Fig. (10)

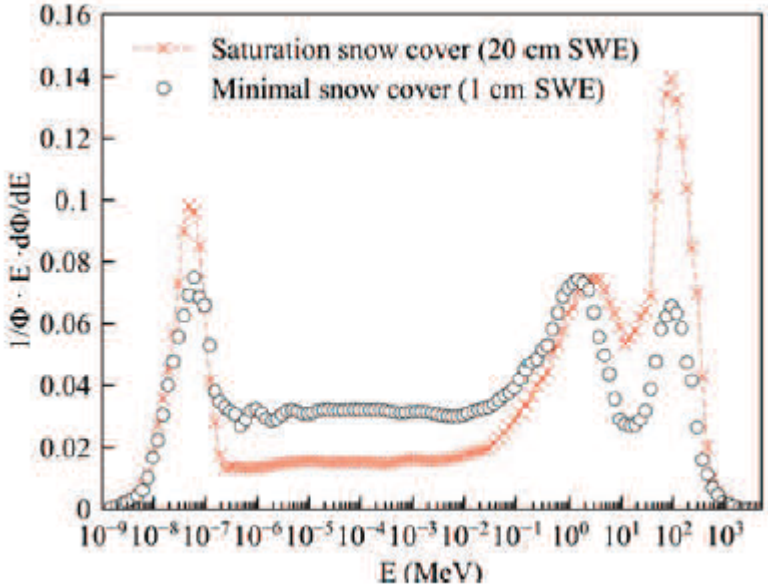

Figure 9: Two guess spectra calculated by Brall *et al.* [4] under "extreme" snow conditions and used to verify the robustness of the unfolding solution. Spectra are normalized to the unit fluence and in lethargy representation.

are specified on a bin-per-bin basis and are obtained by propagating uncertainties on the input quantities (response matrix and sphere counts) through the unfolding process [2], [3]. Interestingly, the uncertainties in the thermal region are large (about $30 \div 40\%$). Indeed, the spectrometer does not include small spheres ($30 \div 50$ mm diameter) that are more sensitive in this region. For practical reasons the number of detectors was limited to eight at design stage, and preference was given to larger spheres to emphasise the resolving power in the more interesting energy region above 10 keV. The thermal peak is only determined by the materials in the vicinity of the system, and is not used to study the properties of the CFG. Nevertheless it is interesting to note that the unfolding process correctly considers the lack of resolving power in this domain by attributing a higher uncertainty to the fluence in the related energy intervals. As expected, the agreement between the two unfolding solutions improves in the epithermal and evaporation regions, where the resolving power is higher and bin-per-bin uncertainties are lower ($10 \div 20\%$). In the cascade region the uncertainties are in the order of $\pm 20\%$ or higher and are mainly due to the larger input uncertainties ($\pm 10\%$) associated to the response of the extended range spheres. These numbers well agree with relevant literature on high-energy response of extended range Bonner Spheres [7]. Tab. (3) reports the spectrum integrated quantities (average between the two solutions of Fig. (10). These data have been corrected:

- For the atmospheric pressure, assuming 671 hPa as a reference pressure for the site;
- For the solar activity, usually represented by the pressure-corrected count rate of the Oulu neutron monitor [8], 6400 min^{-1} was assumed as reference count rate.

Comparing the measured neutron fluence rate with literature values requires prior elaboration. To this aim, literature neutron spectra measured at various elevations but similar latitudes of the Testa Grigia station were elaborated to extract the cascade fluence rate. Fig. (11) reports the

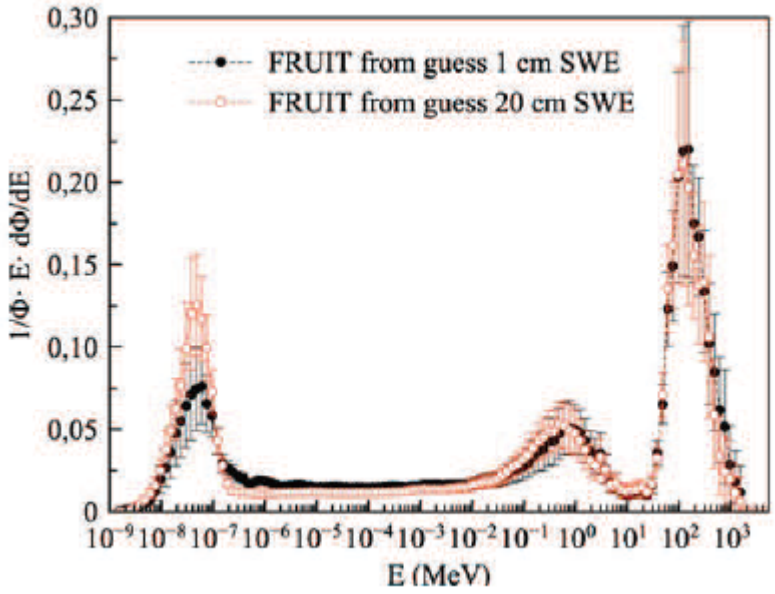

Figure 10: Results of two unfolding sessions using guess spectra with $SWE = 1$ cm and $SWE = 20$ cm (*Snow Water Equivalent*). Spectra are normalized to the unit fluence and in lethargy representation.

corrected cascade fluence rate values as a function of the elevation. The latitude of the sites ranges from 41° 54' (Rome) to to 47° 25' (Zugspitze), corresponding to a vertical geomagnetic rigidity cut-off in the interval $\simeq 4.1 \div 6.3$ GV . Coherently with the results of this work and with relevant literature [7], the fluence rate values were assumed to be affected by a $\pm 20\%$ uncertainty. The experimental values can be fitted by an exponential law of the form:

$$\dot{\phi_C}(z) = \dot{\phi_0} \times \exp \alpha z, \tag{3}$$

where $\dot{\phi_0} = (2.90 \pm 0.20) \times 10^{-3}$ cm^{-2}·s^{-1} and $\alpha = (8.4 \pm 0.5) \times 10^{-4}$ m^{-1} Model-based values obtained with the EXPACS code [9] are also reported in Fig. (11). Interestingly, they closely agree with the exponential fit.

2.3 Conclusion

The cosmic neutron spectrometry campaign at 3480 m in the Testa Grigia Station was successful as it reached the primary objective of validating the extended range Bonner Sphere Spectrometer that will be used by the SAMADHA project to measure neutron fields in the South America. Secondarily, it contributed to increase the available sets of measured neutron spectra at high-elevation sites. These measured data are important because they are used to validate computational models such as those for aircrew dosimetry. Flux variations are expected during the most active phases of the Sun, due the geomagnetic field perturbations or solar proton events, which will be addressed by the future measurements in the Andes within the SAMADHA project.

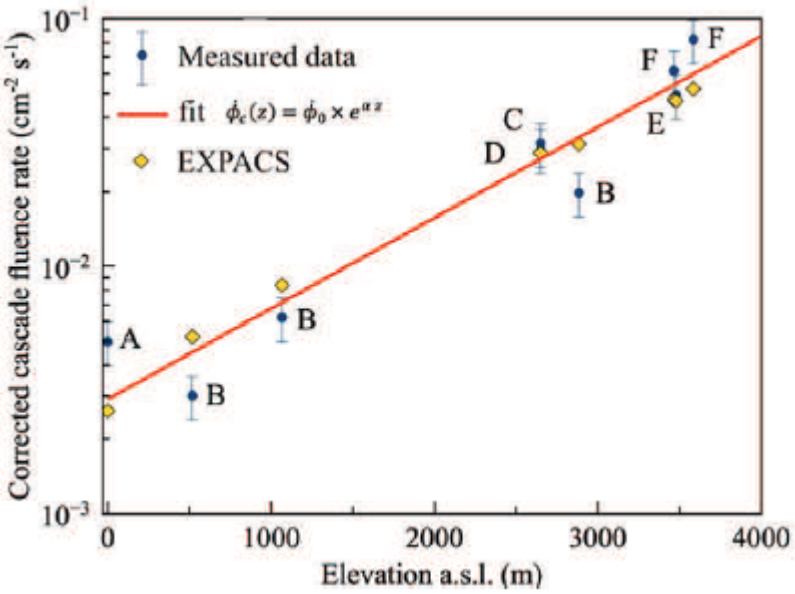

Figure 11: Corrected cascade fluence rate as a function of the elevation. Letters correspond to: (A): Rome at sea level [10], (B) Pic-du-Midi at elevations 518 m, 1067 m and 2885 m [11]; (C) Zugspitze at 2650 m [12]; (D) Zugspitze at 2650 m [13]; (E) This work at 3480 m; (F) Jungfrau at 3475 m and 3585 m [14].

3 FLASHDOS (CNTT)

3.1 Introduction

FLASH radiation therapy is an innovative technique which aims to minimize the damage caused to healthy tissues around a tumour without reducing the efficacy of radiotherapy on the tumour itself. The time of dose delivery is drastically reduced, while the instantaneous dose rate reaches a much higher value than conventional RT.

Flash-RT started out life in 1970's, with the first in-vitro experiment about oxygen depletion in cells irradiated at ultra-high dose rates. In 2014, after 40 years, a report revealed the differential response to high dose rates between normal and tumour tissues in mice.

After this study, a big scientific interest for this new kind of treatment started. Many researchers are using this new technique for experimental tests on both animals and humans.

The radiobiological mechanism discovered and used in this kind of therapy is known as "flash effect", but a complete explication of his causes is still not known.

Current literature indicates that FLASH RT is characterized by a total irradiation duration of less than 200 ms and a dose rate higher than 40 Gy/s (compared to 0.1 Gy/s for conventional RT). Several studies shows that there is a threshold (40 Gy/s according to last results) under which FLASH effect cannot be used.

Clinical accelerators have been developed for this kind of treatment; however, adequate radiation detectors are still not available.

Dosimetry is a fundamental support for a pre-clinical to clinical translation of FLASH RT. Due to the high dose rate delivered during flash radiotherapy, conventional dosimeters have satu-

ration problems and cannot be used for this kind of treatment.

3.2 The UCD dosemeter

The main goal of the TT_FLASHDOS project was the realization of a detector that can be used as a real-time dosemeter for FLASH radiotherapy.

This detector, called UCD (*Unbalanced Core Detector*) is a solid-state dosimeter; only a limited description can be given here due to the ongoing INF patenting process.

It has been manufactured in different shapes and sizes:

- Cylinder with 30 millimetres length and 4 millimetres diameter;
- Sphere with 4, 5 and 6 millimetres diameter.

The acquisition chain is made up of frontend electronics especially designed (current board with automatic selection of the resistance for signal amplification, digitizer and LabView software).

Measurements with flash electron beam at different energy value (7 MeV and 9 MeV) have been carried out in Sordina IORT Technologies s.p.a. (SIT), Aprilia (IT). The ElectronFlash machine is equipped with a 10cm diameter PMMA applicator; the detector was placed in a water phantom and initially centred in the field, as can be seen in figure 1.

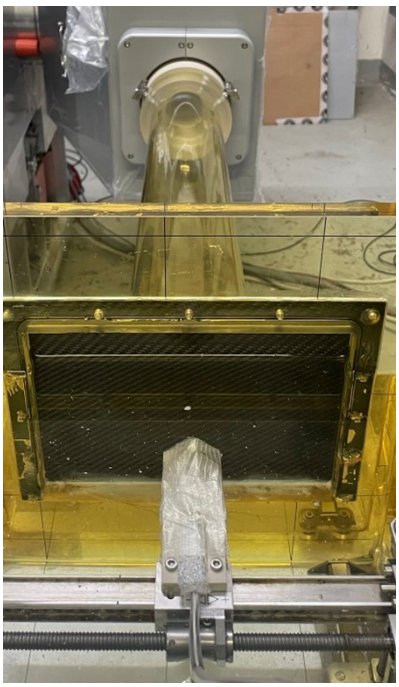

Figure 12: Experimental set-up for measurements carried out in SIT WITH ElectronFlash linac.

The output signal is characterized by 4 microsecond pulses; measured dose is proportional to time-integrated signal.

The following properties of the UCD have been tested in a measurement campaign of about 100 hours:

- Response linearity. The detector is linear up to 26 Gy/pulse, corresponding to instant maximum dose rate of about 6.5 MGy/s;

- Response stability vs. accumulated dose. Damage caused by radiation is negligible, with a fading of 1% after 100 kGy irradiation ;
- Percentage Depth Dose Curves (PDD). There is a great agreement between UCD and Reference diamond detector. In figure 2, an example of PDD curve for 6-mm spherical dosemeter at 7 MeV beam energy is reported. An intrinsic build-up of about 2.5 mm must be subtracted from beam-detector distance due to the intrinsic properties of the detector;
- Lateral Beam Profile. There is an excellent agreement between UCD and Reference diamond detector also in this case. In figure 3, an example of Lateral Beam Profile for 6-mm spherical dosemeter at 7 MeV beam energy is reported;
- Isotropy. Spherical UCD is nearly isotropic.

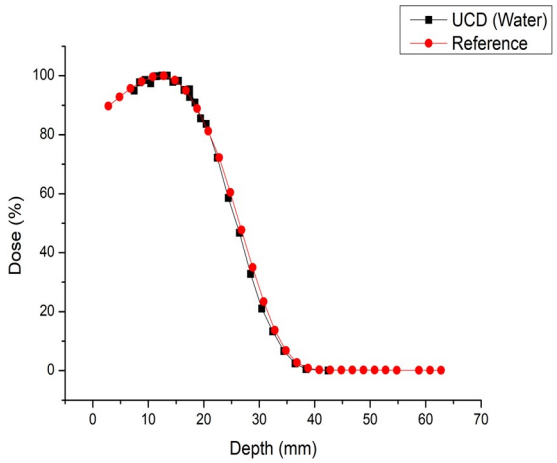

Figure 13: PDD curve for 6-mm spherical UCD and Reference Detector at 7 MeV beam energy.

4 List of Conference Talks by LNF Authors in Year 2022

- R. Bedogni, 6-8 December 2022 Philippine Nuclear Research Institute - 50th *Atomic Energy Week* (AEW) - *Philippine Nuclear Research and Development Conference* PNRDC 2022. Invited talk "Radiation Resistant Neutron and Photon Detectors", Oral;
- L. Russo *et al.*, 30-11-2022 to 02-12-2022, 2nd *Flash Radiotherapy and Particle Therapy Conference* FRPT 2022. Poster "Recent upgrade of UCD, a real-time dosimeter for flash radiotherapy", Poster;
- R. Bedogni, 28th September 2022 NPL, Teddington, UK. NPL Neutron Users meeting. Invited oral " DOIN: a new type of electronic personal neutron dosemeter responding from thermal to 20 MeV neutrons", Oral;
- A. Calamida, 28-30 September 2022, conference AIRP 2022, Milan, talk: "DOIN: un nuovo dosimetro elettronico personale per neutroni", Oral;
- A. Calamida, 14-16 September 2022, conference SISN 2022, Milan, talk: "Extended range Bonner Sphere Spectrometer per misure neutroniche in alta quota", Oral;

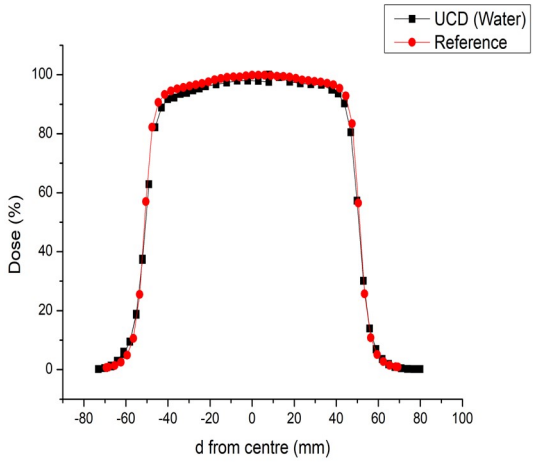

Figure 14: Lateral Beam Profile curve for 6-mm spherical UCD and Reference Detector at 7 MeV beam energy.

- R. Bedogni, 25-29 April 2022 Krakow, Poland. International Conference on Individual Monitoring of Ionising Radiation (IM2022) and Neutron and Ion Dosimetry Symposium (NEUDOS-14), "A single moderator neutron spectrometer for neutron spectrometry in BNCT", Oral;

- A. Calamida *et al.*, 25-29 April 2022 Krakow, Poland. International Conference on Individual Monitoring of Ionising Radiation (IM2022) and Neutron and Ion Dosimetry Symposium (NEUDOS-14), "A new direct-reading neutron personal dosemeter", Poster;

- R. Bedogni *et al.*, 25-29 April 2022 Krakow, Poland. International Conference on Individual Monitoring of Ionising Radiation (IM2022) and Neutron and Ion Dosimetry Symposium (NEUDOS-14) "The Revision of ISO 8529 Neutron reference radiation fields", Poster;

- A. Calamida, 25-29 April 2022 Krakow, Poland. International Conference on Individual Monitoring of Ionising Radiation (IM2022) and Neutron and Ion Dosimetry Symposium (NEUDOS-14)Oral (co-author) "A Bonner Sphere spectrometer for the SAMADHA project", Oral;

- R. Bedogni, 14-18 March 2022 IAEA (*International Atomic Energy Agency*) Vienna. "EVT2104151. Technical Meeting on Best Practices in Boron Neutron Capture Therapy". As "national expert", invited oral "A directional neutron spectrometer for BNCT", Oral.

5 Publications

- R. Bedogni, A. Calamida, A.I. Castro-Campoy, A. Fontanilla, J.M. Gómez-Ros, V. Monti, E. Mafucci, N. Protti, S. Altieri, A. Pietropaolo, *On neutron detection with silicon carbide and its resistance to large accumulated fluence*, Eur. Phys. J. Plus (2022) **137**:1358;

- A. Fontanilla, A. Calamida, I. Castro Campoy, C. Cantone, A. Pietropaolo, J. M. Gomez-Ros, V. Monti, E. Mafucci, S. Vernetto, A. Pola, D. Bortot and R. Bedogni, *Extended range Bonner Sphere Spectrometer for high-elevation neutron measurements*, Eur. Phys. J. Plus (2022) **137**:1315;

- R. Bedogni, A. Calamida, A. Fontanilla, A. I. Castro Campoy, T. Napolitano, C. Cantone, E. Mafucci, V. Monti, S. Altieri, J. M. Gomez-Ros, M. Pillon, A. Pietropaolo, *Measuring the near-target neutron field of a D–D fusion facility with the novel NCT-WES spectrometer*, Eur. Phys. J. Plus (2022) **137**:773.

References

1. National Physical Laboratory, NPL. Test Report N2121(2020020444), 12^{th} August 2022.
2. K. Amgarou *et al.*, Nucl. Instr. Meth. **654**, 399 (2011).
3. S. Agosteo *et al.*, Nucl. Instr. Meth. A **694**, 55 (2012).
4. T. Brall *et al.*, Radiat. Meas. 144, 106592 (2021).
5. A. Fontanilla *et al.*, EPJ-Plus **137(12)**, 1315 (2022).
6. C. Pioch *et al.*, Rad. Meas. **45**, 1263 (2010).
7. W. R*ü*hm *et al.*, Rad. Meas. **67**, 24 (2014).
8. M. Bittner, Science at the environmental research station Schneefernerhaus/ Zugspitze (Umwelt Forschungsstation Schneefernerhaus, 2022).
9. T. Sato, EXPACS PLOS ONE **10** (2015).
10. J. Gòmez-Ros *et al.*, Radiat. Meas. **106**, 580 (2017).
11. A. Cheminet *et al.*, IEEE Trans. Nucl. Sci. **59**, 1722 (2012).
12. A. Zimbal and other, Proceed. NEUDOS-11. (2009).
13. V. Mares, private comm..
14. V. Mares *et al.*, Rad. Phys. Chem. **168**, 262 (2020).